Silver Nanoparticles Synthesized Using *Carica papaya* Leaf Extract (AgNPs-PLE) Causes Cell Cycle Arrest and Apoptosis in Human Prostate (DU145) Cancer Cells

Surya P. Singh[1] · Abhijeet Mishra[2] · Ritis K. Shyanti[2] · Rana P. Singh[2] · Arbind Acharya[1]

Abstract

Treatment of cancer has been limited by the poor efficacy and toxicity profiles of available drugs. There is a growing demand to develop alternative approaches to combat cancer such as use of nano-formulation-based drugs. Here, we report biosynthesis and characterization of silver nanoparticles (AgNPs) with papaya leaf extract (PLE) and its anti-cancer properties against different human cancer cells. Purified nanoparticles were characterized by standard techniques, such as TEM, STM, SEM, EDS, XRD, and FTIR. Furthermore, cytotoxic activity of AgNPs-PLE was carried out against different human cancer cells and non-tumorigenic human keratinocytes cells. AgNPs-PLE when compared with AgNPs-citric acid or PLE showed better efficacy against cancer cells and was also relatively less toxic to normal cells. Treatment of DU145 cells with AgNPs-PLE (0.5–5.0 μg/ml) for 24–48 h lowered total cell number by 24–36% ($P < 0.05$). Inhibition of cell growth was linked with arrest of cell cycle at G2/M phase at 24 h, while G1 and G2/M phase arrests at 48 h. ROS production was observed at earlier time points in presence of AgNPs-PLE, suggesting its role behind apoptosis in DU145 cells. Induction of apoptosis (57%) was revealed by AO/EB staining in DU145 cells along with induction of Bax, cleaved caspase-3, and cleaved PARP proteins. G1-S phase cell cycle check point marker, cyclin D1 was down-regulated along with an increase in cip1/p21 and kip1/p27 tumor suppressor proteins by AgNPs-PLE. These findings suggest the anti-cancer properties of AgNPs-PLE.

Keywords *Carica papaya* leaf extracts · Silver nanoparticles · Anticancer · Prostate cancer · Apoptosis

Introduction

There were 8.2 million cancer-related deaths and 32.6 million people living with cancer [1]. Incidences of new cancer cases are estimated to increase by 70% in the coming 2 decades [2]. Among different cancers, lung cancer has the highest incidence and mortality rate in both male and female [3, 4]. In addition, breast cancer is also leading cause of death in female followed by prostate cancer in male. Around 40,920 deaths of women are estimated in the USA alone in 2018 [3, 5]. Approximately, 20% of death was due to prostate cancer among men especially in America, while in Europe, it is one of the most frequent cancers in the year 2018 [6]. Currently,

various systemic treatments are employed such as surgery, chemotherapy, radiotherapy, and hormone therapy; however, mortality and morbidity could not be reduced [7, 8]. In addition, these therapeutics are linked to severe side effects such as toxicity to normal cells/tissues, vomiting, nausea and hair loss, and development of resistance [9, 10]. With the aim to avoid these undesirable effects, many medicinal and herbal plant extracts have been investigated for their potential antitumor activities [11]. Although plant extracts or phytochemicals could potentiate cancer treatment, there are some limitations such as bioavailability and poor solubility [12]. In this context, nano-biotechnology could play a noteworthy role to overcome the limitations of conventional treatment strategies.

Advantages associated with green synthesized eco-friendly and biocompatible silver nanoparticles using fungi, bacteria, and plants have larger scope when compared with the conventional method for metallic nanoparticles preparation [13–16]. Furthermore, green synthesis using plants appears to be faster and is able to produce quite rapidly AgNPs compared with bacteria and fungi [17]. Plant extracts have outstanding properties for the fabrication of metal-based nanoparticles such as

✉ Arbind Acharya
   acharya@bhu.ac.in

[1] Department of Zoology, Banaras Hindu University, Varanasi, UP, India

[2] Cancer and Radiation Biology Laboratory, School of Life Sciences, Jawaharlal Nehru University, New Delhi, India

silver and gold [18–20]. However, the constituents which are the key players in plant extracts that lead to the synthesis of nanostructure are yet to be established [21]. Synthesis of nanoparticles mediated by plant extract is more beneficial as the tedious process of cell-mediated biotransformation can be skipped and would be suitable for large scale production in addition to being simplistic, lower cost, environment friendly, and safe for human therapeutics [18]. Among different types of nanoparticles, AgNPs being used as therapeutic agent against various diseases such as anti-parasitic, anti-malarial, bactericidal, fungicidal, and anti-cancer [22]. Plant extracts have already been used successfully for the biosynthesis of AgNPs [22–28]. The higher surface area to volume ratio of the AgNPs is predictable to increase its cytotoxic activity. Therefore, smaller size of AgNPs showed greater penetration ability than the larger one and cause more toxicity to cancer cells [29, 30].

AgNPs synthesized with various plant materials have shown anti-cancer effects against the lung cancer A549 cells [31], lymphoma mouse model [23], MCF-7 cells [32], human cervical carcinoma cells [33], Dalton's lymphoma (DL) cells and colon adenocarcinoma Colo205 [34], and human hepatoma HepG2 cells [35]. Recent meta-analysis study based on green synthesized nanoparticles using microbial or plant extracts had shown promising anti-cancer effects against different types of cancer cells with negligible toxic impact on normal cells [36]. Biosynthesis of AgNPs (size ranged from 2 to 20 nm) using neem leaf extract and its cytotoxic activity against human cervical cancer cells (SiHa) has been evaluated [16]. Recently, He and colleagues [37] have shown biosynthesis of AgNPs using peel extract of *Dimocarpus longan* Lour and evaluated its cytotoxicity on human prostate cancer PC-3 cells. Otsuki and co-workers reported the effect of *Carica papaya* extract on the enhanced production of Th1 type cytokines from human lymphocytes [38]. Furthermore, the leaf extract of papaya was reported to suppress the growth of oral squamous cell carcinoma (SCC25) cells [39]. The previous study has been reported that biosynthesis of silver nanoparticles by using *Carica papaya* leaf having antibacterial activity [40], but its effect on molecular changes in the prostate cancer cells is unexplored yet.

Herein, AgNPs were synthesized using papaya leaf extract (PLE) and investigated for its anti-cancer potential against various human epithelial cancer cells including prostate carcinoma (DU145), lung carcinoma (A549), breast carcinoma (MCF-7), and epidermoid carcinoma (A431) cells together with a non-tumorigenic HaCaT cells. To the best of our knowledge, this is the first study to (i) evaluate its anti-cancer potential against various cancer cells and (ii) explore the associated biological events in prostate cancer cells.

Materials and Methods

Materials

Fresh leaves of papaya were obtained from the Jawaharlal Nehru University campus, New Delhi. Silver nitrate was purchased from Merck India Ltd. Other chemicals and solvents used were of analytical grade.

Preparation of *Carica papaya* Leaf Extract (PLE)

Healthy fresh *Carica papaya* leaves were collected from average height of female plant. Collected leaves were washed multiple times with tap water followed by distilled water. Whole leaves were allowed to get air-dried and grinded using mortar and pestle to get powder. Every 20 g of leaf powder was mixed with 400 ml of water and kept at 60 °C until 50 ml water is left. Extracts were subsequently filtered through using Whatman filter paper followed by 0.22-µm filter (MILLIPORE) and stored at 4 °C. This sterile aqueous papaya leaf extract was used further for the synthesis of AgNPs-PLE.

Synthesis of Silver Nanoparticles Using Citric Acid

Silver nanoparticles were synthesized by the reduction of silver nitrate solution and initiated by mixing of aqueous solution of $AgNO_3$ (1 mM) and citric acid (2.5 mM) and by heating the reaction solution (100 °C) with continuous stirring on the magnetic stirrer as described earlier with slight modification [41]. Synthesis of silver nanoparticles was monitored by UV-visible spectroscopy.

Fabrication of AgNPs with Papaya Leaf Extract

Fabrication of the AgNPs was done by mixing 200 µl of aqueous solution of papaya leaf extract in 10 ml of freshly prepared silver nitrate solution (1 mM). Solution was incubated in water bath at 50 °C, while pH value of solution was 8. Aliquot was taken at regular time interval and the biosynthesis of AgNPs was observed by UV-vis spectroscopy (300-900 nm) (Hitachi spectrophotometer 625) ran at a resolution of 1 nm. $AgNO_3$ and papaya leaf extract (PLE) solution were used as controls. The fabrication of AgNPs was similarly investigated as a function of time, concentrations of PLE and silver ions, and pH.

Purification of AgNPs-Citric Acid and AgNPs-PLE

The AgNPs were isolated and purified as reported earlier [42]. Briefly, AgNPs were isolated after completion of reaction using centrifugation (5000 rpm, 15 min, 4 °C). The obtained supernatant was removed carefully and the pellet was washed four times with MQ water, to ensure removal of all Ag + ions.

Further pellet was air-dried and used for characterization studies [43]. Different concentrations of AgNPs-PLE were prepared for biological studies as described earlier [44].

Characterization of AgNPs-Citric Acid and AgNPs-PLE

Characterizations of AgNPs-PLE were carried out by methods as reported earlier [44, 45], and detailed below.

UV-vis Spectroscopy Primary characterization of the AgNPs-citric acid and AgNPs-PLE synthesis process was carried out using UV-vis spectroscopy (Hitachi spectrophotometer 625) worked at a resolution of 1 nm. The bioreduction of silver ions (Ag^+) to silver atom ($Ag^°$) was monitored by measuring the spectra of the reaction medium at regular intermission.

Transmission Electron Microscopy Briefly, sample for transmission electron microscopy (TEM) was prepared by drop coating of sonicated solution of AgNPs-citric acid and AgNPs-PLE on to the carbon coated copper TEM grids. TEM measurements were accomplished on a JEOL, F2100 instrument operated at an accelerating voltage at 200 kV.

Scanning Electron Microscopy Scanning electron microscopy (SEM) images were obtained using an EVO 40 instrument (ZEISS, Germany). The sample was placed on a carbon tape and then coated with a thin layer of gold using a sputter coater. An Energy-Dispersive X-ray spectroscopy (EDS) spectrum was taken along with SEM for elemental analysis of above prepared sample.

Scanning Tunneling Microscopy Scanning tunneling microscopy (STM) was carried out using Nanosurf Easyscan 2 (Switzerland) working in air at room temperature. The sample for STM was prepared by suspending 1 mg of dry powder of AgNPs-PLE in 10 ml of ethanol. After sonication, a drop of the solution was put on platinum coated substrate. The sample was examined after air drying under STM microscope. For this experiment, constant current mode was used.

Fourier-Transform Infrared Spectroscopy Spectra of AgNPs-PLE and papaya leaf extract were recorded on a Fourier-transform infrared spectroscopy (FTIR) spectrometer (PerkinElmer). FTIR spectroscopy was obtained using KBr pellets. In order to obtain good signal to noise ratio, thirty-two scans of samples were taken in the range 400–4000 cm^{-1} and the resolution was kept as 4.0 cm^{-1}.

X-ray Diffraction X-ray diffraction (XRD) spectrum of AgNPs-PLE was recorded by X'Pert Pro X-ray diffractometer (PANanlytical BV) by operating X-ray tube at 45 kV and 35 mA, and the radiation used was Cu-Kα.

Cell Culture and Treatment

Human prostate carcinoma (DU145), lung carcinoma (A549), breast carcinoma (MCF-7), skin carcinoma (A431), and human keratinocytes (HaCaT) cells were obtained from ATCC (Manassas, VA). First three cell lines were grown as adherent monolayer in RPMI 1640 (Roswell Park Memorial Institute) media (Himedia Laboratories) added with fetal bovine serum (10%) and penicillin-streptomycin (1%), while A431, HaCaT cells cultured and maintained in DMEM medium supplemented with 10% fetal bovine serum (Gibco™ Fetal Bovine Serum, qualified, Brazil) and 1% penicillin-streptomycin. Cells were cultured at 37 °C and 95% humidified incubator with 5% CO_2, and maintained by sub-culturing the cells twice a week. All the cells were treated with different concentration of AgNPs-PLE (0.5, 1, 2.5, and 5 μg/ml of medium) for 24 and 48 h whereas PBS was used as control.

Cell Growth and Viability Assays

DU145 cells were seeded at 1×10^5 in each 60-mm culture dishes and incubated at 37 °C overnight. Furthermore, cells were treated with different concentrations of the AgNPs-PLE (0, 0.5, 1, 2.5, and 5 μg/ml medium) for 24 h and 48 h. After desired treatments, the attached cells were removed after brief trypsinization and washed with PBS twice, then gently mixed with trypan blue dye and counted using hemocytometer as described earlier [46]. Trypan blue determines viable and dead cells. Each set of treatment was done in triplicates and the experiment was repeated twice. Furthermore, MTT assay was carried out to assess the growth inhibitory effect of AgNPs-PLE, on DU145, A549, MCF-7 A431, cells as described earlier [16]. In another set of experiment, DU145 and HaCaT cells were treated at concentration of the PLE, AgNPs-citric acid, and AgNPs-PLE (5 μg/ml) for 24 h, and MTT assay was performed.

Flow Cytometry Analysis of Cell Cycle Progression

DU145 cells were seeded likewise as cell growth and viability assay and treated with AgNPs-PLE. At the completion of each treatment, total cells were collected and processed for cell cycle analysis as reported earlier [47]. The cell suspension prepared from the treated plates was centrifuged at 1500 rpm for 5 min. The supernatant was removed and the pellet was washed with PBS buffer and re-suspended in 0.5 ml saponin-propidium iodide (PI) cocktail solution [0.3% saponin (w/v), 25 mg/ml PI (w/v), 0.1 mM EDTA, and 10 mg/ml RNase A (w/v) in PBS buffer] in dark. All tubes were incubated at 4 °C for overnight in dark. The data was acquired using the CellQuest software in a FACS Calibur (Becton Dickinson, USA) for 10,000 events per sample and analyzed

using the Win MDI software after suitable gating, to know the cell percentage in each phase of the cell cycle.

ROS Measurement

To measure ROS production, DU145 cells were seeded at a density of 8×10^3 cells per well in 96-well culture plate. After 24 h, cells were pretreated with 10 μM DCFHDA reagent and incubated for 30 min. DCFHDA was removed and washed twice with serum free media. NAC treatment was given at a concentration of 5 mM for 5 h prior to H_2O_2 and AgNPs-PLE (2.5 and 5 μg/ml) exposure. Further ROS production was measured by a multi-plate reader (Varioskan Flash, Thermo Scientific) in terms of fluorescence intensity (excitation filter at 485 nm and emission filter at 530 nm) at 30 min, 1 h, 3 h, 6 h, 12 h, and 24 h respectively [48].

Quantification of Apoptotic Cells by Acridine Orange/Ethidium Bromide Staining

DU145 cells were seeded at a density of 1×10^5 cells per 60-mm culture plate. Cells were treated with 0.5, 1, 2.5, and 5 μg/ml concentrations of AgNPs-PLE in the culture medium. After the treatment periods, i.e., 24 h and 48 h, cells were collected by trypsinization. Twenty-five microliters of each cell suspension was aliquoted into a microcentrifuge tube placed on ice. One microliter of a dye mixture containing of 100 μg/ml acridine orange (AO) and 100 μg/ml ethidium bromide (EtBr) prepared in PBS buffer was mixed to cell suspension. Ten microliters of the dye-cell mixture was visualized under a fluorescent microscope (Nikon Eclipse Ti-S; Nikon Corp., Tokyo, Japan) and pictures were taken at × 200 using a blue filter for AO stain, green filter for EtBr stain and later both images were merged for a final image as reported earlier [49].

Cell Lysis and Immunoblotting

At the end of the treatment, cells were lysed with cell lysis buffer (containing protease and phosphatase inhibitors) to obtain whole cell lysate protein. Quantification of the protein was done by Bradford method and 50 μg of protein per lane was loaded on a 12% SDS-PAGE, resolved, and transferred onto PVDF membrane. To detect the expression of different proteins, the membrane was incubated with the specific primary and their respective secondary antibodies. Anti-Cyclin D1 was obtained from Santa Cruz Biotechnology, USA, whereas anti-p21, anti-p27, anti-Bax, anti-cleaved caspase-3, and anti-cleaved PARP antibodies were purchased from Cell Signaling Technology, USA. The secondary antibodies for anti-mouse and anti-rabbit were procured from Sigma Aldrich. The blots were developed using enhanced

chemiluminescence from Merck Millipore (Billerica, MA) and the exposure was captured on X-ray film [50].

Statistical Analysis

Results were statistically analyzed using GraphPad prism version 5 as mean ± standard error of experiment performed in triplicates. Statistical differences were evaluated using a one-way analysis of variance (ANOVA) with Dunnett's test or Bonferroni's multiple comparison test. Differences were considered to be statistically significant at a level of $P < 0.05$.

Results

Synthesis and Characterization of AgNPs-Citric Acid and AgNPs-PLE

The UV-visible spectroscopy confirmed synthesis of silver nanoparticles using citric acid (Fig. 1a). Absorption maxima at 419 nm revealed controlled shape and size of synthesized nanoparticles. Optical property of AgNPs-PLE was periodically analyzed using UV–vis spectroscopy. The absorption spectrum of AgNPs-PLE solution was originated due to the surface plasmon resonance (SPR) [44]. In order to get desired size and shape of AgNPs, optimization of parameters during synthesis is a crucial step. When the extract of papaya leaves was slowly mixed with the freshly prepared silver nitrate solution, the solution turned into brown in color within 15 min (inset of Fig. 1b). The silver SPR centered at 427 nm with increasing intensity until 120 min (Fig. 1b). However, at 135 min, a small reduction in absorption intensity was observed. This tendency is attributed to the aggregation of nanoparticles during biosynthesis and is consistent with earlier reports [44, 51].

Another important parameter which affects the formation of AgNPs-PLE was the concentration of PLE. The reaction solutions containing 50 μl, 300 μl, and 400 μl of PLE with 1 mM silver nitrate solution developed a light yellow brown color, while those containing, 100 μl and 200 μl of PLE developed darker reddish-brown color (inset of fig. 1c). The peak of SPR of AgNPs-PLE was comparably intense and the sharp peak intensity was found at 200 μl of PLE (Fig. 1c). When the concentration of the leaf extract increased, the AgNPs-PLE synthesis was also increased, but at higher concentration of the leaf extract decrease in the synthesis was observed. Mishra and colleagues (2013) have shown that the ratio of phytoconstituent molecules influences the AgNP formation. Similar reports were also observed with *Azadirachta indica* (Neem) leaf extract [52], and Ashoka leaf extract [44]. Variation in the metal-salt concentration is also identified to effect nanoparticle synthesis [53]. However, in our study, the concentration of silver ions
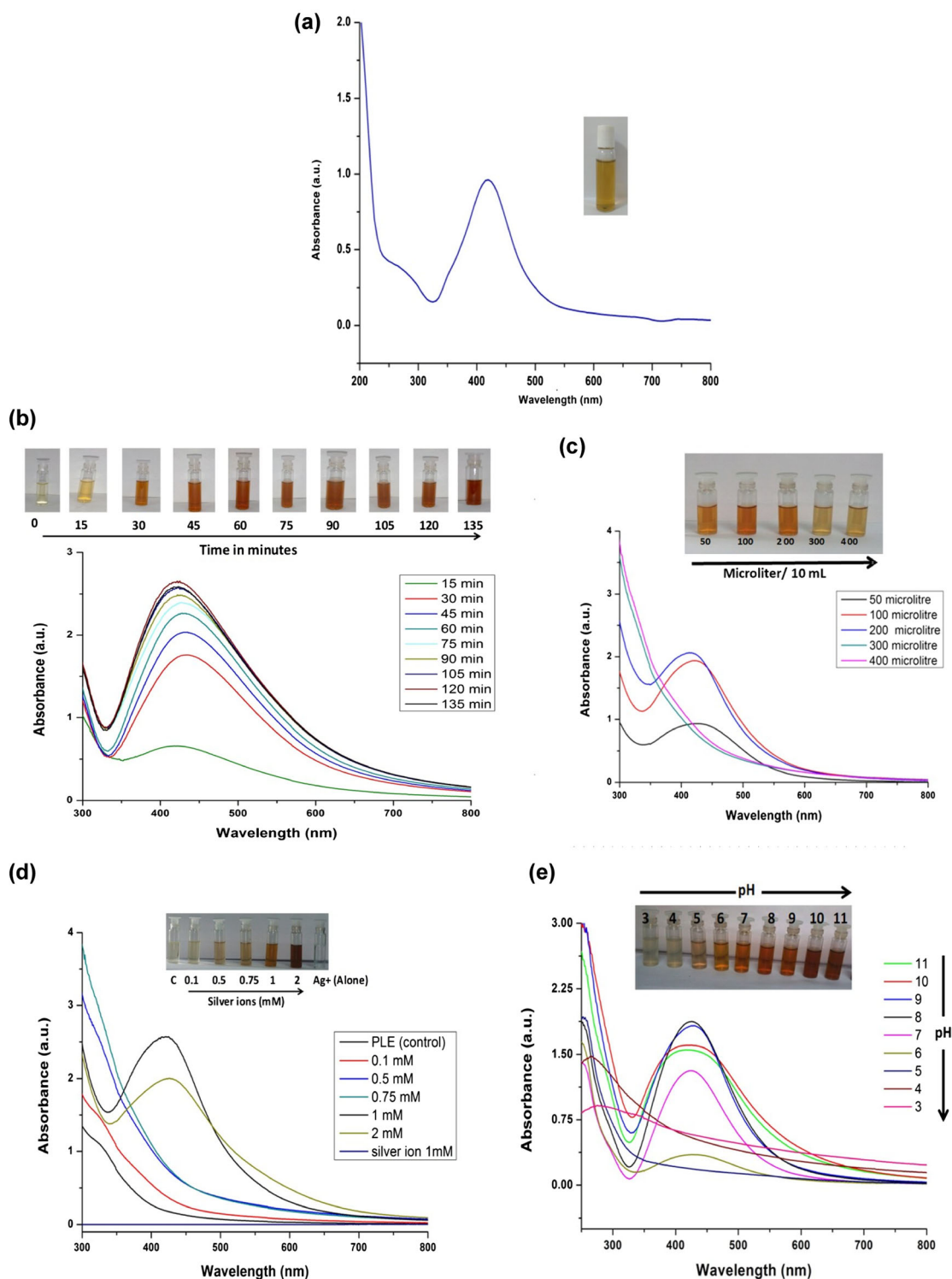
Fig. 1 **a** Synthesis of silver nanoparticles (AgNPs) using citric acid alone. **b** Optimization of AgNPs synthesis by PLE. Effect of incubation time: UV-vis spectra analysis of AgNPs-PLE synthesized at various time intervals i.e. from 15 to 135 min. **c** Effect of PLE concentration: The concentration of the leaf extract was varied from 50 µl to 400 µl per 10 mL of reaction volume. **d** Effect of silver ion concentration: the concentration of silver ion ranges from 0.1 to 2 mM. **e** Effect of pH: UV-vis spectral analysis of the AgNPs-PLE at various pH (3 to 11)

for synthesis of AgNPs-PLE was also observed as a crucial parameter. When silver salt concentrations of 0.1 mM, 0.5 mM, 0.75 mM, 1 mM, and 2 mM mixed and incubated

with the PLE solution separately, yellowish-brown and light-brown colors were noticed at silver salt (AgNO₃) concentrations of 0.1 and 0.5 mM, while reddish-brown color with
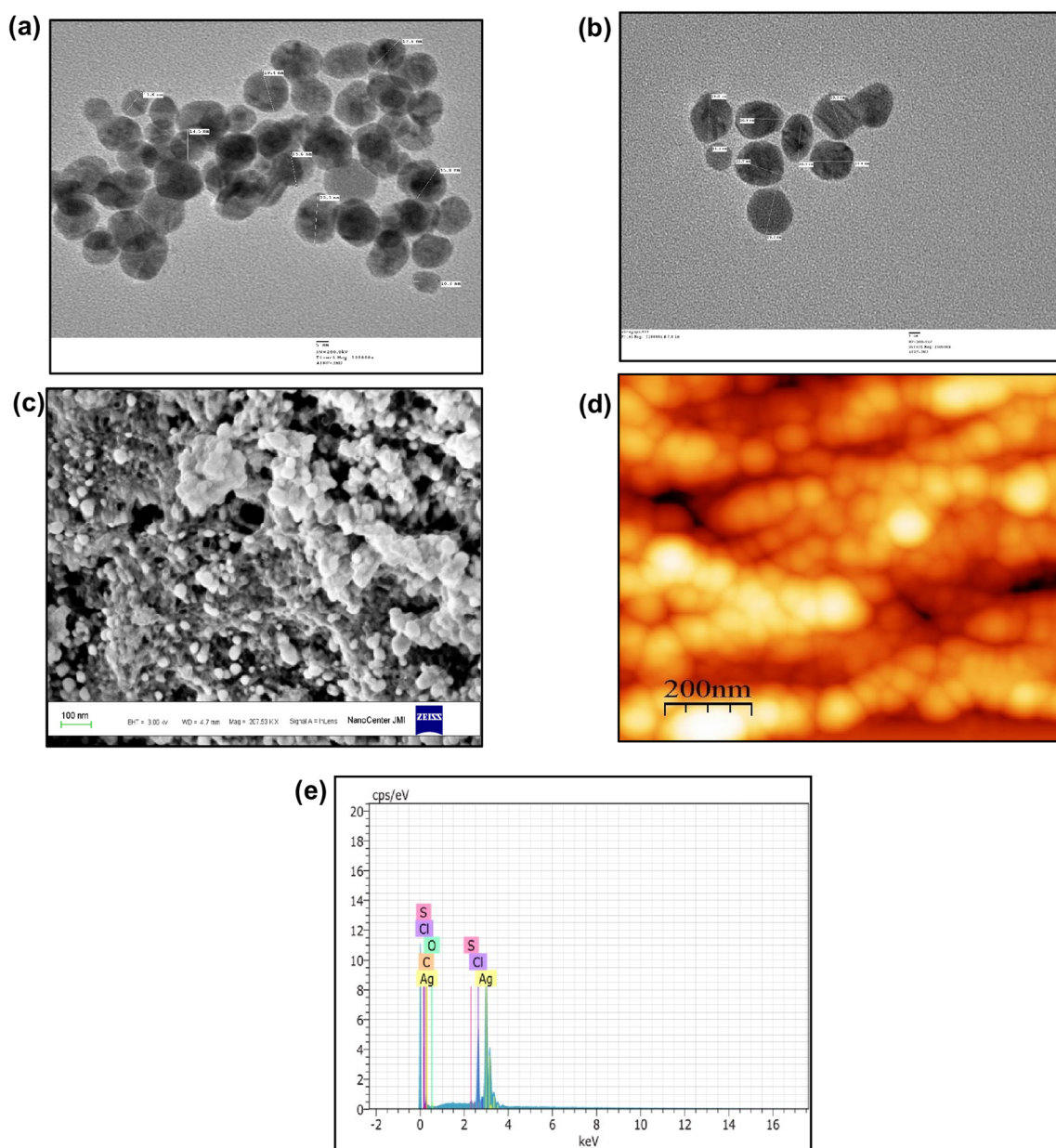
Fig. 2 a TEM image of AgNPs-citric acid and AgNPs-PLE. b Sample was prepared by drop coating of sonicated solution of AgNPs-PLE on to carbon coated copper TEM grids. TEM measurements were operated at an accelerating voltage at 200 kV. c STM image of AgNPs-PLE. The sample for STM was prepared by suspending 1 mg of dry powder of AgNPs-PLE in 10 ml of ethanol. The sample was examined after air drying under STM microscope. For this experiment, constant current mode was used. d SEM micrograph of AgNPs-PLE. Images were obtained using an EVO 40 instrument (ZEISS, Germany). The sample was placed on a carbon tape and then coated with a thin layer of gold using a sputter coater. e EDS of AgNPs-PLE. An EDS spectrum was taken along with SEM for elemental analysis

darker shades was observed at 1.0 to 2.0 mM concentrations of silver salt (inset of Fig. 1d). The SPR spectra of AgNPs-PLE became more distinctive with increased silver salt concentration and the maximum peak absorbance was attained at 1 mM of silver ions (Fig. 1d).

Change in the pH of solution influences the size and shape of the nanoparticles. Charge of biomolecules could be altered after change in pH, which might affect their capping and stabilizing capabilities during synthesis of nanoparticles.

Intensity and color of reaction mixture were pH-dependent as reported earlier [36, 44]. When the biosynthesis of AgNPs-PLE was carried out at pH 3.0 and 4.0, neither considerable change in color nor characteristic SPR spectra of AgNPs-PLE was obtained (inset of Fig. 1e), while at pH values of 6.0 and 7.0, a gradual increase in the intensity of color of solution was observed. Maximum absorbance was observed at pH 8.0 (Fig. 1e). When pH of reaction solution varied from 9.0 to 11.0, SPR peaks were decreased due to
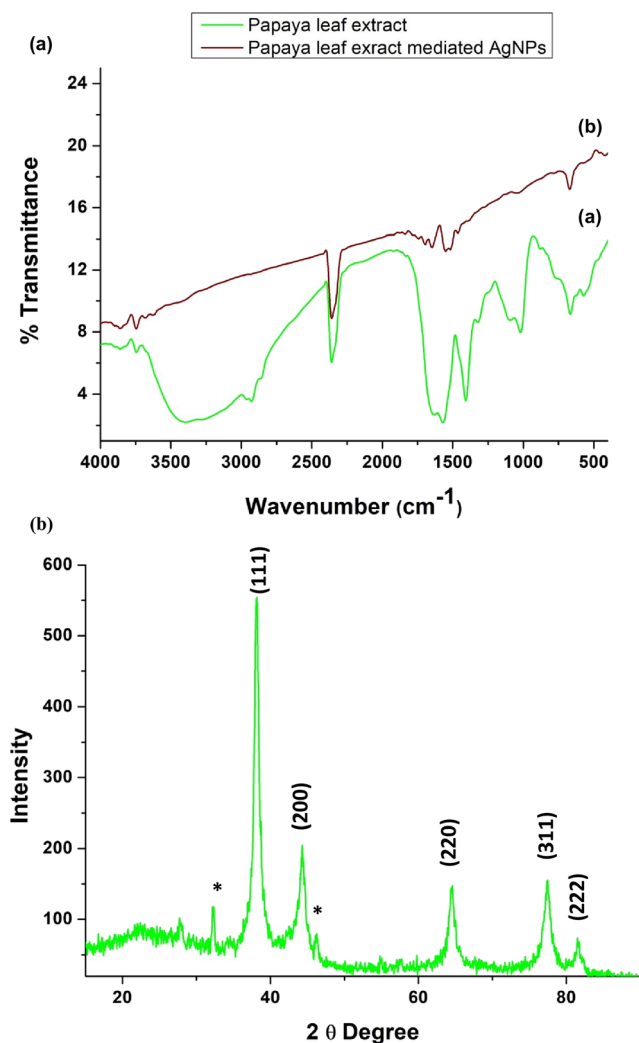
Fig. 3 **a** FTIR spectra of PLE and AgNPs-PLE.FTIR spectroscopy was done using KBr pellets. To obtain good signal to noise ratio, 32 scans of AgNPs-PLE were taken in the range 400–4000 cm^{-1}and the resolution was kept as4.0 cm^{-1}. **b** X-ray diffraction of powdered AgNPs-PLE.XRD spectrum of AgNPs-PLE was recorded by X'Pert Pro X-ray diffractometer (PANanlytical BV) by operating X-ray tube at 45 kV and 35 mA, and the radiation used was Cu-Kα

change in the charges of biomolecules. Our results were also supported by the earlier reports [36, 54].

Microscopic Characterization TEM analysis of chemically synthesized AgNPs-citric acid was observed round in shape and range between 10 and 25 nm (Fig. 2a). The size and shape of AgNPs-PLE were analyzed using TEM, STM, and SEM. Sizes of the AgNPs-PLE estimated from TEM image were in the range of 10–20 nm (Fig. 2b). The images captured of AgNPs-PLE using STM (Fig. 2c) showed that the surface is smooth and spherical. STM data analysis also showed a good agreement with the TEM analysis. The SEM micrographs of AgNPs-PLE were analyzed to observe the topographical characteristics and shape. SEM data analysis shown particles are almost spherical in shape with uniform distribution (Fig. 2d).

Spectroscopic Characterization EDS analysis of the AgNPs-PLE revealed the presence of silver (Ag), oxygen (O), sulfur (S), and chlorine (Cl) elements (Fig. 2e). Carbon peak was also observed which would be due to its presence in the grid [55]. It has been already reported that AgNPs neem leaf extract synthesized were bound by a thin layer of capping organic material [56]. In order to know the possible role of biomolecules during synthesis of AgNPs, FTIR of PLE and AgNPs-PLE were carried out. FTIR spectra analysis showed the presence of different functional groups which existed on AgNPs-PLE and crude *C. papaya* leaf extract (Fig. 3a). It can be observed that, in contrast to the extract, the AgNPs-PLE showed significant changes in their respective vibrational spectrum. The absorption peaks at 3745and 3318 cm^{-1}were observed in the leaf extract due to OH stretching vibration, which could not be observed in the AgNPs-PLE. Absorbance is accredited to N–H or C=O stretching vibration band indicating the presence of flavonoids or proteins [57]. The band showing at 1646 cm^{-1} was present in the AgNPs-PLE and papaya leaf extract which corresponds to the C–N stretching of amide I bands or phenols/amines or aliphatic amines [57]. The infrared bands at 1565 and 1411 cm^{-1} were characteristics of amide bond [58]. To know the crystalline nature of AgNPs-PLE, we further carried out XRD. The XRD analysis of the purified powdered particles showed Bragg's reflections which is the characteristic of metallic silver nanoparticles (Fig. 3b). The data showed diffraction peaks at 2θ values 32.173°, 38.039°, 64.393°, 77.358°, and 81.55°, corresponding to the (111), (200), (220), (311), and (222) planes of AgNPs-PLE in a cubic phase, respectively. Two unassigned peaks (marked with star) were observed in the XRD spectrum of AgNPs-PLE and it may be due to the crystallization of bioorganic phase during synthesis of the AgNPs-PLE. Our findings were also supported by the earlier published studies [56, 59].

AgNPs-PLE Inhibits Growth and Survival of Various Epithelial Cancer Cells

To study the cytotoxic effect of AgNPs-PLE, DU154, A549, MCF-7, A431 cells were treated with different concentrations of AgNPs-PLE for 24 h and MTT assay was performed (Fig. 4a–d). Result shows that treatment with 5 μg/ml AgNPs-PLE decreases cell viability by 74% in DU145 cells, 29% in A549 cells, 51% in MCF-7 cells, and 36% in A431 cells. In previous report, silver ion showed hemolytic activity up to 10 μg/ml, while plant extract mediated AgNPs showed no hemolytic activity up to 40 μg/ml [44]. On the basis of this observation, we further treated DU145 and HaCaT cells with 5 μg/ml AgNPs-PLE, PLE, and AgNPs-citric acid for 24 h and determined cell viability. AgNPs-PLE showed more significant cytotoxic effect on DU145 compared with PLE or AgNPs,

Fig. 4 Effect of AgNPs-PLE on cell viability of **a** human prostate cancer DU145, **b** lung cancer A549, **c** breast cancer MCF-7, and **d** skin cancer A431 cells by MTT assay. Cells were treated with 0, 0.5, 1, 2.5, and 5 μg/ml of AgNPs-PLE for 24 h. Cells were processed for MTT assay as per standard protocol. Furthermore, **e** DU145 and **f** HaCaT cells were treated with 5 μg/ml concentrations of PLE or AgNPs-citric acid or AgNPs-PLE for 24 h followed by MTT assay. #$P < 0.001$ compared with control
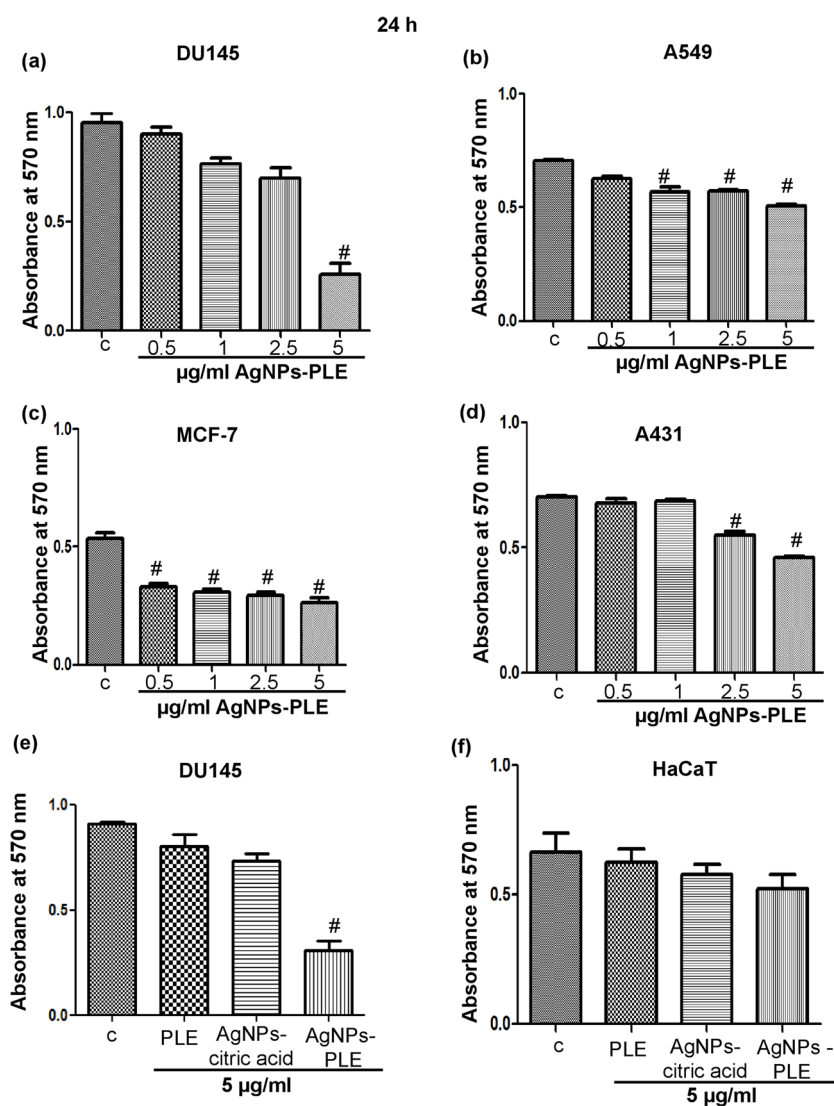
while non-tumorigenic HaCaT cells did not show significant decrease in cell viability (Fig. 4e and f). This finding suggests that the AgNPs-PLE would be therapeutically more suitable than PLE or AgNPs-citric acid, and therefore, DU145 cells were selected for further study with AgNPs-PLE.

Effects of AgNPs-PLE on Proliferation and Viability of Human Prostate Cancer Cells

On the basis of MTT data, we further evaluated the growth inhibitory efficacy of AgNPs-PLE on human prostate carcinoma DU145 cells. It was observed that treatment with AgNPs-PLE (0.5, 1, 2.5, 5 μg/ml) at 24 h and 48 h reduced the cell proliferation and lead to cell death in a dose-dependent manner (Fig. 5). At 24 h, a decrease in the total cell number of 17–24% ($P < 0.0001$) and induced cell death up to 2.5–5.8% ($P < 0.05$) was observed after treatment with AgNPs-PLE (Fig. 5a and b), whereas after 48 h of treatment, a decrease in the cell number of 36% ($P < 0.05$) and an increase in cell

death up to 16% ($P < 0.0001$) were observed (Fig. 5c and d). These results suggest that AgNPs-PLE have potential to inhibit cell proliferation and induce cell death in DU145 cells.

AgNPs-PLE Induced Cell Cycle Arrest in Prostate Cancer Cells

Induction of cell cycle arrest is one of the mechanisms of decreased cell proliferation by various anti-cancer agents. We explored the effects of AgNPs-PLE on cancer cell cycle progression, when DU145 cells were treated with different concentrations of AgNPs-PLE (0.5–5 μg/ml) (Fig. 6). We observed that G2/M phase of cell cycle arrests at both 24 h and 48 h time points in response to the higher dose of AgNPs-PLE (5 μg/ml) (Fig. 6a and b), while at 48 h time point, G1 phase arrest occurred in presence of lower doses of AgNPs-PLE (0.5, 1, and 2.5 μg/ml) (Fig. 6c and d). Western blotting data showed decreased level of cyclin D1 and increased levels of cip1/p21 and kip1/p27 expression in presence of AgNPs-

Fig. 5 Effect of AgNPs-PLE on cell growth and death on human prostate carcinoma DU145 cells. Cells were treated with 0.5–5 μg/ml of AgNPs-PLEfor24 h and 48 h, and total cells were counted using a hemocytometer, and dead cells were scored using trypan blue dye exclusion method. For 24 h treatment: **a** total cell number and **b** dead cells. For 48 h treatment: **c** total cell number and **d** dead cells. *$P < 0.05$, #$P < 0.001$ compared with control
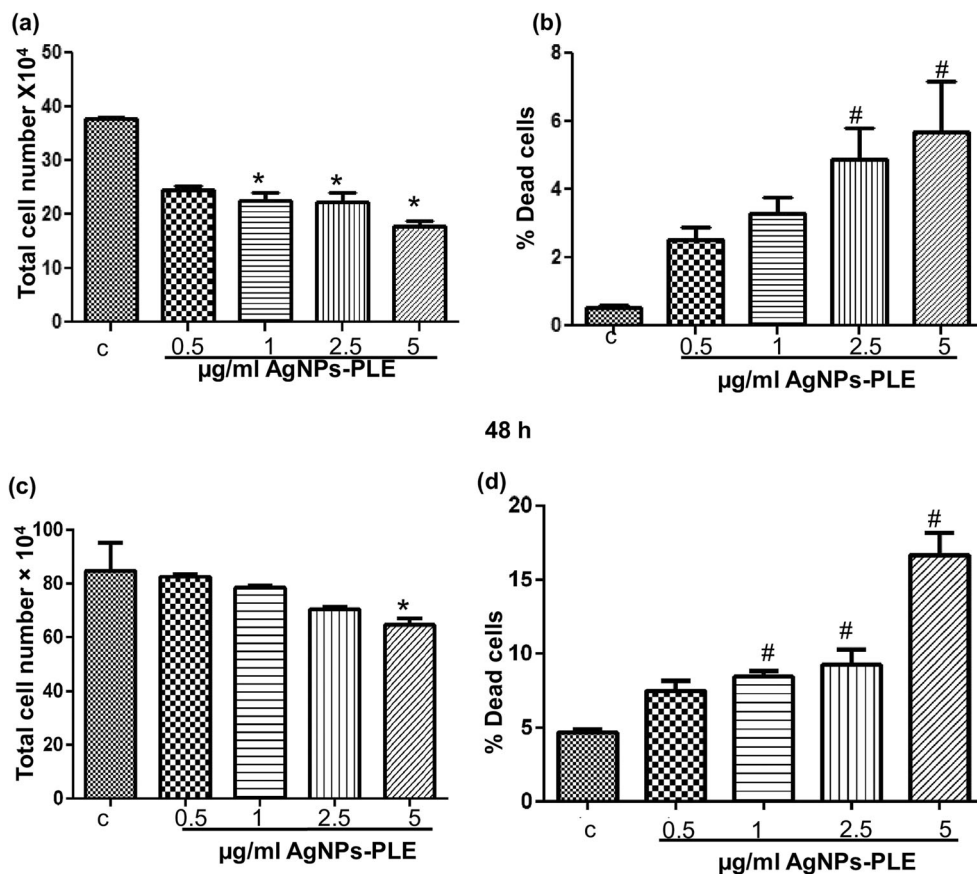
PLE compared with the control (Fig. 9a).These molecular changes in presence of AgNPs-PLE further suggest its role on cell cycle arrests resulting in inhibition of growth and proliferation of cancer cells.

AgNPs-PLE Induced Intracellular ROS Generation in Prostate Cancer Cells

ROS formation is known to be one of the phenomena in apoptosis induction; therefore, we examined whether ROS contributed in AgNPs-PLE induced apoptosis in DU145 cells. To quantify the level of ROS generation, we performed DCFHDA assay [39, 60]. We observed concentration-dependent AgNPs-PLE mediated increased ROS generation at very early time points such as 30 min and 1 h (Fig. 7a and b). The positive control H_2O_2 sequentially induced ROS generation at all the time points. We also observed the anti-oxidant effect of NAC inhibited the ROS generation (Fig. 7a–f).

## AgNPs-PLE Induced Apoptosis in Prostate Cancer Cells

To determine, whether the inhibition of cancer cell proliferation by AgNPs-PLE was in part due to the induction of apoptosis, we used AO/EtBr staining of cells to quantify the apoptotic cells. Figure 8 summarizes the apoptotic effects of AgNPs-PLE in DU145 cells. A dose-dependent increase in apoptosis was clearly observed when cells were treated with 0.5, 1, 2.5, and 5 μg/ml of AgNPs-PLE for 24 h and 48 h. When compared with the control, 50% and 57% of the cell population in 5 μg/ml AgNPs treated cells displayed apoptosis after treatment of 24 h and 48 h, respectively (Fig. 8a and b). Furthermore, we studied the effect of AgNPs-PLE on apoptotic markers through western blotting, and the protein levels of cleaved-caspase-3 (17 kDa and 19 kDa) and cleaved-PARP (89 kDa) molecules were upregulated significantly compared with the control (Fig. 9b). Elevated level of Bax, a pro-apoptotic molecule, was also found in the treated cells as compared to the control (Fig. 9c), suggesting the apoptotic effect of AgNPs-PLE on cancer cells.

Discussion

In the last decade, the synthesis of silver nanoparticles using plant extracts is getting more attention due to their application in biomedical sciences such as anti-parasitic, anti-malarial, bactericidal, and fungicidal including anti-cancer activity [20, 22, 61]. Nanoparticles in different shapes and sizes have been reported for anti-cancer activities both in vivo and

Fig. 6 Effect of AgNPs-PLE on cell cycle arrest in DU145 cells. Cells were treated with 0.5– 5 μg/ml of AgNPs-PLE for 24 h and 48 h, then collected and incubated overnight with saponin/ PI solution at 4 °C and analyzed by flow cytometer as detailed in materials and methods. **a** and **c** Representative diagrams and **b** and **d** quantitative cell cycle phase distribution data for 24 and 48 h of treatments, respectively. Results are representative of three independent experiments. *$P < 0.05$ compared with control
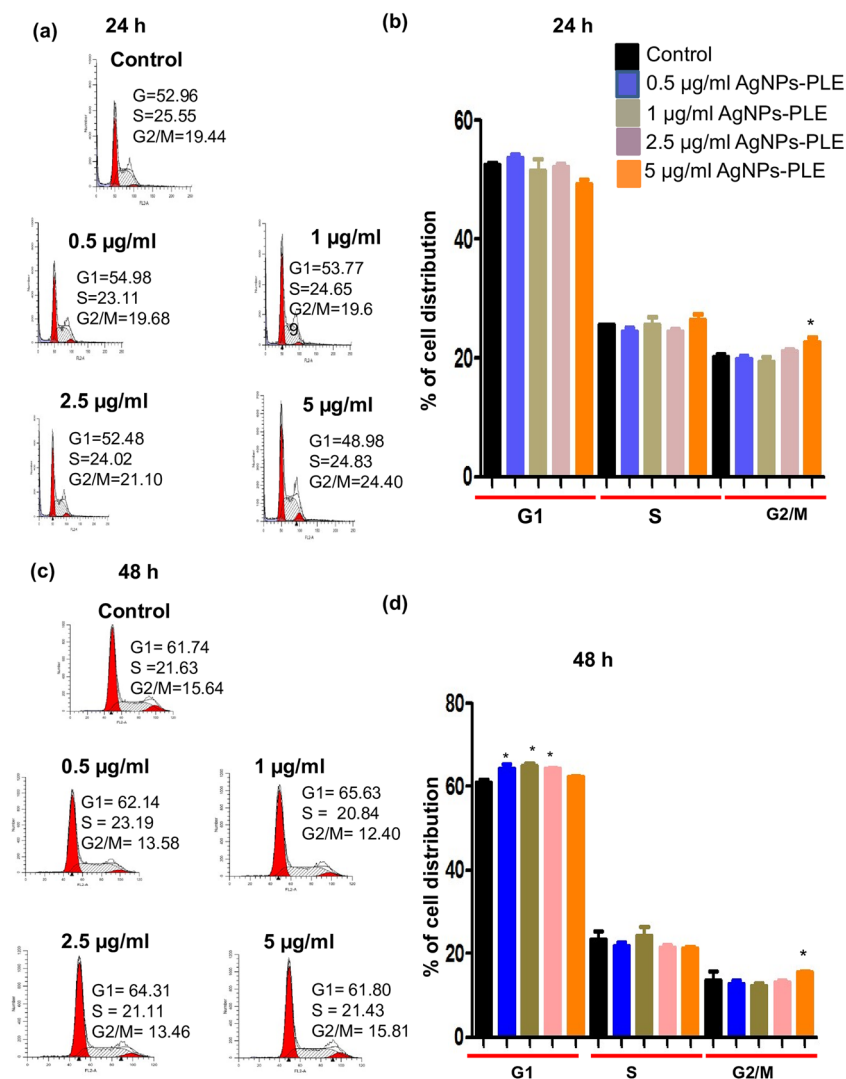
in vitro. In the current scenario, green synthesized nanoparticles are at focused area due to its biocompatibility nature and exhibiting better cytotoxicity towards cancer cells. There are several reports in making a desirable (size and shape), stable, environmental friendly nanoparticles by applying variations in concentration, pH, temperature [4, 44]. Moreover, anti-tumor activity of different types of green synthesized NPs such as gold, silver, or graphene oxide has been documented against 3T3 mouse fibroblasts, A549 lung cancer, HCT116 colorectal cancer, and Hep-2 laryngeal carcinoma. Most of the cases, it is the nanoparticles formed better compared with the base (tyrosine, catalase, diastase) used for green synthesis significantly affecting the cytotoxic potentials against cancer cells of different origin [5, 59, 61–63] .

In the present study, we have synthesized and characterized AgNPs with *Carica papaya* leaf extract (PLE) and investigated its anti-proliferative, cell cycle, and apoptosis effects on cancer cells. For the synthesis of AgNPs-PLE, it is essential to control not only the size of nanoparticles but also the

distribution and shape as well. Large numbers of studies are going on exploring the anti-cancer aspects of green synthesized nanoparticles. There are few reports where possible side effects of such nanoparticles were discussed may vary case wise depending upon the method applied, biological sources taken, or conditions of synthesis [64, 65]. Therefore, we have tried to optimize our green nanoparticle synthesis approach in order to overcome the above limitations associated with anti-cancer therapeutics. PLE was prepared as discussed in the "Materials and Method" section, while in control experiments, the UV-visible spectra of silver nitrate solution and PLE were taken; they did not show any peak indicating that leaf extract was accountable for the synthesis of AgNPs. Characterization of nanoparticles using standard techniques is necessary to ensure its purity, effectiveness, and acceptability [66]. Microscopy techniques such as TEM, STM, and SEM were carried out to know the size, shape, and surface characteristics such as topography and porosity of AgNPs-PLE. Size of AgNPs-PLE ranged from 10 to 20 nm and was spherical in
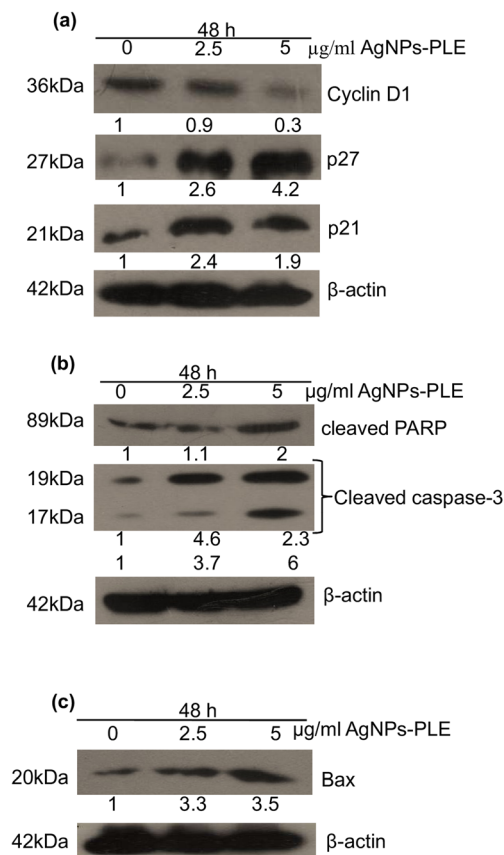
Fig. 9 Effect of AgNPs-PLE on the expression of apoptosis and anti-proliferative molecular mediators. Western blotting was done in DU145 cells treated with 2.5 and 5 μg/ml AgNPs-PLE and untreated control for 48 h. **a** Representative images showing expression of cyclin D1, kip1/p27, cip1/p21, and β-actin as loading control. **b** Protein level expression of cleaved PARP (89 kDa), cleaved caspase-3 (17 kDa and 19 kDa), and loading control β-actin. **c** Images representing the protein expression of Bax, (20 kDa) and the loading control β-actin. Densitometric value of each protein is quantified using Image J software and mentioned below each band as fold change of control

shape. The EDS spectrum recorded from the AgNPs-PLE along with SEM. The EDS analysis showed strong signal of silver that confirms the existence of metallic silver [42]. Apart from silver peak, we also observed the presence of trace element such as S, Cl, and O, which may be originated from the biomolecules present in PLE bound to the surface of the AgNPs.

FTIR spectroscopy data clearly indicates that biomolecules present in papaya leaf extract were having major role for the synthesis and stabilization of AgNPs. Papaya leaf extract contains alkaloids, polyphenols, and flavonoids [38, 67]; therefore, we can speculate that these molecules were served as reducing and capping agent for the AgNP synthesis. In fact, these molecules have antioxidant properties which particularly help in the reduction of silver ions to silver atoms. The key mechanism is the hydrogen abstraction from OH groups which is usually present in the polyphenol molecules [68]. Crystal structure and phase purity of AgNPs

have been evaluated by XRD. The XRD spectrum of powdered AgNPs confirmed the crystalline nature. All the peaks shown in XRD graph of AgNPs can be attributed to cubic structure of metallic silver as per existing literature (JCPDS, File No. 4-0783).

In the present study, we explored the anti-cancer activity of synthesized AgNPs-PLE on various human epithelial cancer cells and found maximum cytotoxicity in DU145 cells compared with the other cancer cells. More importantly, it showed relatively very less toxicity to HaCaT normal cells. Furthermore, anti-cancer activity of AgNPs-PLE was assessed in DU145 cells by using trypan blue assay that showed growth inhibitory activity accompanied with an increase in the population of dead cells. Increased proliferation and unregulated growth of cell are major hallmarks of cancer [46]. Development of cancer is associated with uncontrolled cell cycle and it is one of the most significant cellular events which are usually observed in cancer cells [47]. We found that treatment of AgNPs-PLE on DU145 cells showed G2/M and G1 arrests in cell cycle progression. Molecules that are involved in cell cycle progression and regulation play crucial role in maintaining routine growth of various type of cells [69].

The cell cycle check-point regulators such as cyclin and cyclin-dependent kinase and their protein expression and activities describe the fundamental status of cells and fate of cell proliferation. Our western blotting data for cyclin D1 protein expression, a regulator of G1-S phase transition, was significantly down-regulated in AgNPs-PLE treated DU145 cancer cells which were in concurrence with the previous studies reporting G1 cell cycle arrest [70]. p21/cip1, a universal CDK inhibitor, and p27/kip1 belong to Cip/Kip family proteins that regulate the activity of cyclins and CDKs and thereby responsible for controlling cell proliferation wherein p21 and p27 expressions are linked to anti-cancer signals [71]. These two important CDK inhibitors are upregulated during cell cycle arrest mediated through different anti-cancer agents [70, 72, 73]. An important anti-tumor event such as decreased cyclin D1 and the increased p21/cip1 and p27/kip1 were mediated by AgNPs-PLE treatment in DU145 cells.

There are evidences of cancer cells undergoing apoptosis due to ROS generation i.e., group of short-lived, highly reactive, oxygen-containing molecules in the presence of anti-tumor agents [48, 60, 74]. DCFHDA results suggesting ROS events occurring in presence of AgNPs-PLE at earlier time points may be playing role behind apoptosis process in DU145 prostate cancer cells. Generally, resistance to apoptosis is a key defect in cancer cells. Induction of apoptosis is mainly characterized by the few factors including cell shrinkage, nuclear condensation, and DNA fragmentation. In the present study, our data showed that treatment with AgNPs-PLE causes apoptosis as a mechanism of cell death in DU145 cells. To understand initiation of apoptosis in DU145 cells, AO/EtBr assay was performed. AO is a dye which can stain

Fig. 7 Intracellular ROS generation in AgNPs-PLE treated human prostate cancer DU145 cells. ROS production was measured by DCFDA assay at 30 min, 1 h, 3 h, 6 h, 12 h, and 24 h time points. **a**, **b**, **c**, **d**, **e**. and **f** Cells were treated with either DMSO (control) or 2.5 and 5 μg/ml AgNPs-PLE. Initially, cells were treated with DCFDA (10 μM) followed by NAC (5 mM) treatment. H_2O_2 (2 μM) was taken as positive control to measure the intracellular ROS production and the fluorescence was noted at respective time points (**a**–**f**) as detailed in the "Materials and Methods" section. Columns mean triplicate samples; bars, SD experiment was repeated twice with similar findings. *($P < 0.05$), **($P < 0.01$), #($P < 0.001$). The P value is obtained by comparing control group with each treatment group and between the treated groups using one-way ANOVA followed by Bonferroni's Multiple Comparison Test
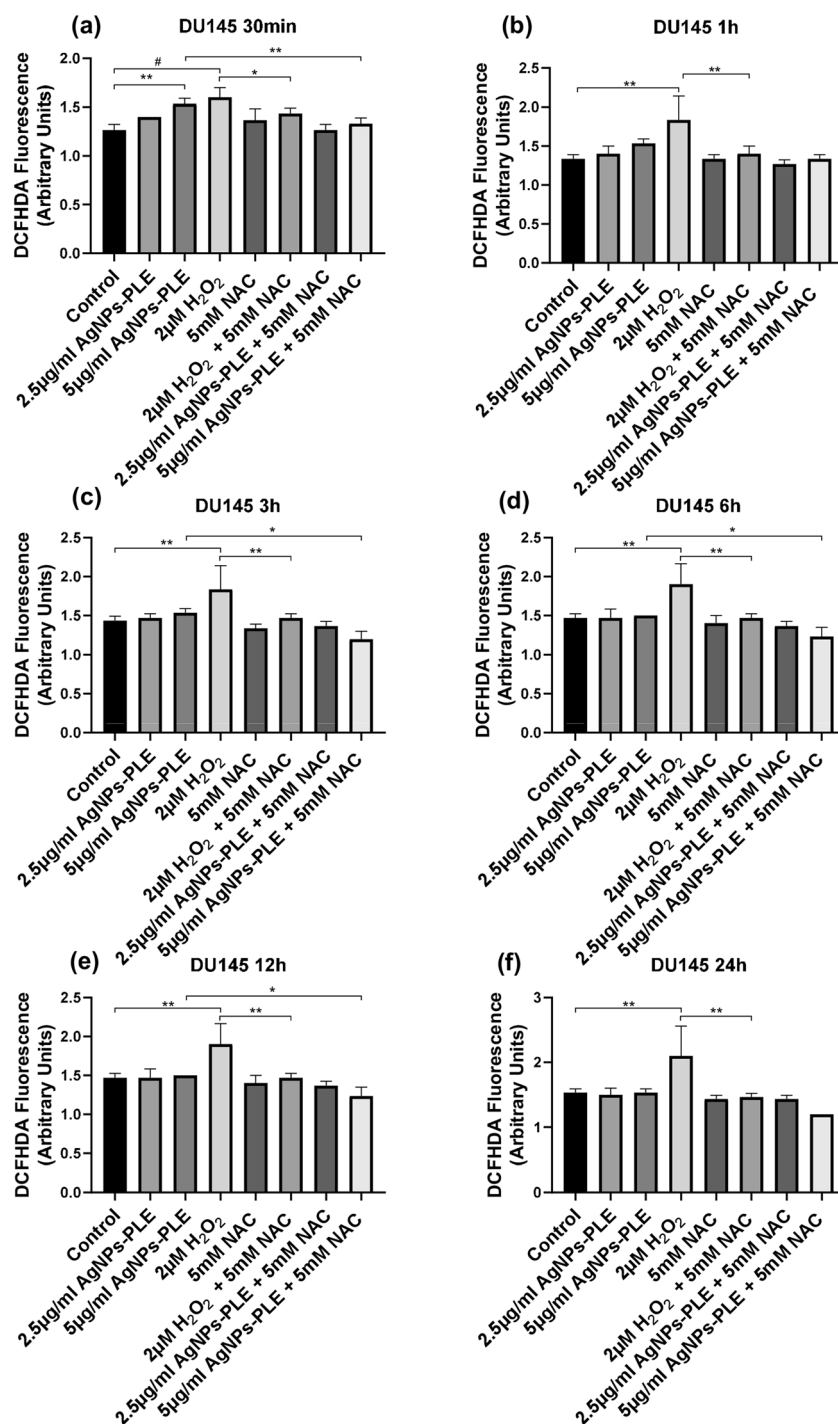
both live and as dead cells, while EtBr can only stain those cells which lost their membrane structure and integrity. Uniformly green cells are live cells and can be readily differentiated from apoptotic cells as they show yellow-orange and necrotic cells exhibit red color which is dependent on the amount of loss of membrane integrity [49]. Further western blotting results of increased expression levels of cleaved PARP and cleaved caspase-3 mediated by AgNPs-PLE further confirm the occurrence of apoptotic events in DU145

prostate cancer cells. Another pro-apoptotic marker Bax was also found to be significantly upregulated after AgNPs-PLE treatment. These results are also supported by other studies reporting apoptosis in various treatment conditions [50, 71, 75, 76]. Overall, our results indicated that biosynthesized AgNPs-PLE inhibit growth of human prostate cancer cells involving cell cycle arrest and apoptotic cell death and therefore could be a potential anti-cancer candidate against epithelial or prostate cancer cells.

Fig. 8 AO/EtBr staining of DU145 cells to detect apoptosis induced by AgNPs-PLE. **a** Live cells are uniformly green, whereas apoptotic cells and necrotic cells are characterized by yellow-orange and red staining, respectively, due to chromatin condensation and loss of membrane integrity. **b** Quantitative percent apoptotic cell data for 24 h of treatment of AgNPs-PLE. **c** Quantitative percent apoptotic cell data for 48 h of treatment of AgNPs-PLE. *$P < 0.05$ compared with control
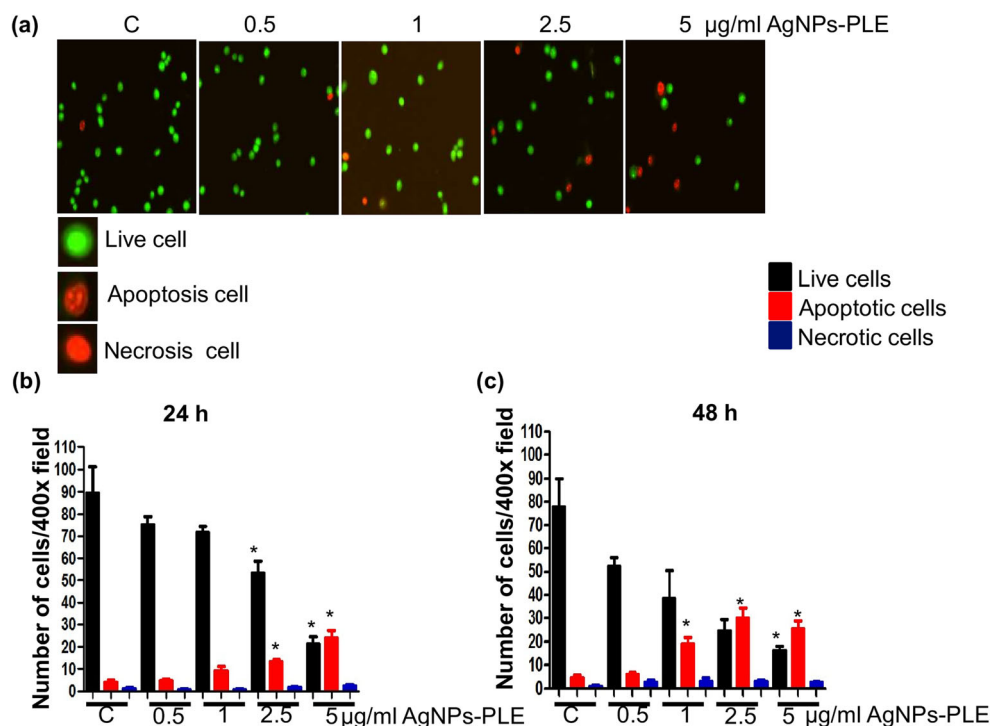
Conclusions

The present study reports that biosynthesis of AgNPs with *Carica papaya* leaf extract (PLE) which is cost-effective, eco-friendly, an alternative route of synthesis, and with promising strong and selective anti-cancer activity against prostate cancer cells. Microscopic analysis of nanoparticles showed that the size ranged from 10 to 20 nm and spherical in shape. XRD data revealed crystalline nature of nanoparticles. In addition, AgNPs-PLE showed anti-cancer activity against the lung, breast, and epidermoid carcinoma cells. The anti-cancer activity is associated with cell cycle arrest and apoptosis may be due to the consequences of increased ROS production by AgNPs-PLE. After exploring the majority of cell growth and cell death molecules at protein levels of Cyclin D1, p21, p27, Caspases, and Bax, PARP further indicates the anti-tumor potential of green synthesized AgNPs-PLE in vitro. There were certain limitations of AgNPs where the cytotoxic concentrations against cancer cells also found to be cytotoxic for normal cells. In this context, our findings of AgNPs-PLE concentrations used for anti-tumor effects are quite safer when compared with a normal cell line HaCaT. Based on the encouraging in vitro findings in the present study, in vivo animal studies could be carried to further establish AgNPs-PLE as a potential drug candidate to treat and control epithelial cancers including prostate cancer.

Compliance with Ethical Standards

Conflict of Interest The authors declare that they have no conflict of interest.

Ethical Approval This article does not contain any studies with human participants or animals performed by any of the authors.

References

1. Siegel RL, Miller KD, Jemal A (2019) Cancer statistics, 2019. CA Cancer J Clin 69:7–34
2. Stewart B, Wild CP (2015) World cancer report 2014 world
3. Barabadi H, Hosseini O, Kamali KD, Shoushtari FJ, Rashedi M, Haghi-Aminjan H, Saravanan M (2020) Emerging theranostic silver nanomaterials to combat lung cancer: a systematic review. J Clust Sci 31:1–10
4. Vahidi H, Barabadi H, Saravanan M (2020) Emerging selenium nanoparticles to combat cancer: a systematic review. J Clust Sci 31:301–309
5. Barabadi H, Mahjoub MA, Tajani B, Ahmadi A, Junejo Y, Saravanan M (2019) Emerging theranostic biogenic silver nanomaterials for breast cancer: a systematic review. J Clust Sci 30:259–279
6. Barabadi H, Kamali KD, Shoushtari FJ, Tajani B, Mahjoub MA, Alizadeh A, Saravanan M (2019) Emerging theranostic silver and gold nanomaterials to combat prostate cancer: a systematic review. J Clust Sci 30:1375–1382. https://doi.org/10.1007/s10876-019-01588-7

7. Palumbo MO, Kavan P, Miller WH Jr, Panasci L, Assouline S, Johnson N, Cohen V, Patenaude F, Pollak M, Jagoe RT, Batist G (2013) Systemic cancer therapy: achievements and challenges that lie ahead. Front Pharmacol 4:1–9

8. Casanovas O (2012) Limitations of therapies exposed. Nature 484: 44–46

9. Coates A, Abraham S, Kaye SB, Sowerbutts T, Frewin C, Fox RM, Tattersall MH (1983) On the receiving end–patient perception of the side-effects of cancer chemotherapy. Eur J Cancer Clin Oncol 19:203–208

10. Szakács G, Paterson JK, Ludwig JA, Booth-Genthe C, Gottesman MM (2006) Targeting multidrug resistance in cancer. Nat Rev Drug Discov 5:219–234

11. Cai Y, Luo Q, Sun M, Corke H (2004) Antioxidant activity and phenolic compounds of 112 traditional Chinese medicinal plants associated with anticancer. Life Sci 74(17):2157–2184

12. Aqil F, Munagala R, Jeyabalan J, Vadhanam MV (2013) Bioavailability of phytochemicals and its enhancement by drug delivery systems. Cancer Lett 334(1):133–141

13. Barabadi H, Tajani B, Moradi M, Kamali KD, Meena R, Honary S, Mahjoub MA, Saravanan M (2019) Penicillium family as emerging nanofactory for biosynthesis of green nanomaterials: a journey into the world of microorganisms. J Clust Sci 30:843–856

14. Kanagamani K, Muthukrishnan P, Shankar K, Kathiresan A, Barabadi H, Saravanan M (2019) Antimicrobial, cytotoxicity and photocatalytic degradation of norfloxacin using Kleinia grandiflora mediated silver nanoparticles. J Clust Sci 30(6):1415–1424

15. Rehman S, Farooq R, Jermy R, Asiri SM, Ravinayagam V, Jindan RA, Alsalem Z, Shah MA, Reshi Z, Sabit H, Khan FA (2020) A Wild Fomes fomentarius for biomediation of one pot synthesis of titanium oxide and silver nanoparticles for antibacterial and anticancer application. Biomolecules 10(4):1–15

16. Subbaiya R, Saravanan M, Priya AR, Shankar KR, Selvam M, Ovais M, Balajee R, Barabadi H (2017) Biomimetic synthesis of silver nanoparticles from Streptomyces atrovirens and their potential anticancer activity against human breast cancer cells. IET Nanobiotechnol 11(8):965–972

17. Rauwel P, Küünal S, Ferdov S, Rauwel E (2015) A review on the green synthesis of silver nanoparticles and their morphologies studied via TEM. Adv Mater Sci Eng 2015:1–9

18. Thakkar KN, Mhatre SS, Parikh RY (2010) Biological synthesis of metallic nanoparticles. Nanomedecine 6(2):257–262

19. Kumar V, Yadav SK (2009) Plant-mediated synthesis of silver and gold nanoparticles and their applications. J Chem Technol Biotechnol 84(2):151–157

20. Shankar SS, Rai A, Ankamwar B, Singh A, Ahmad A, Sastry M (2004) Biologicalsynthesis of triangular gold nanoprisms. Nat Mater 3(7):482–488

21. Chauhan A, Zubair S, Sherwani A, Owais M (2012) Aloe vera induced biomimetic assemblage of nucleobase into nanosized particles. PLoS One 7(3):e32049

22. Honary S, Barabadi H, Ebrahimi P, Naghibi F, Alizadeh A (2015) Development and optimization of biometal nanoparticles by using mathematical methodology: a microbial approach. JNanoR 30: 106–115

23. Boomi P, Poorani GP, Palanisamy S, Selvam S, Ramanathan G, Ravikumar S, Barabadi H, Prabu HG, Jeyakanthan J, Saravanan M (2019) Evaluation of antibacterial and anticancer potential of polyaniline-bimetal nanocomposites synthesized from chemical reduction method. J Clust Sci 30(3):715–726

24. Barabadi H, Alizadeh Z, Rahimi MT, Barac A, Maraolo AE, Robertson LJ, Masjedi A, Shahrivar F, Ahmadpour E (2019) Nanobiotechnology as an emerging approach to combat malaria: a systematic review. Nanomedicine 18:221–233

25. Prabhu D, Arulvasu C, Babu G, Manikandan R, Srinivasan P (2013) Biologically synthesized green silver nanoparticles from leaf extract of Vitex negundo L. induce growth-inhibitory effect on human colon cancer cell line HCT15. Process Biochem 48(2): 317–324

26. Jeyaraj M, Sathishkumar G, Sivanandhan G, MubarakAli D, Rajesh M, Arun R, Kapildev G, Manickavasagam M, Thajuddin N, Premkumar K, Ganapathi A (2013) Biogenic silver nanoparticles for cancer treatment: an experimental report. Colloids Surf B: Biointerfaces 106:86–92

27. Lokina S, Stephen A, Kaviyarasan V, Arulvasu C, Narayanan V (2014) Cytotoxicity and antimicrobial activities of green synthesized silver nanoparticles. Eur J Med Chem 76:256–263

28. Ulug B, Haluk Turkdemir M, Cicek A, Mete A (2015) Role of irradiation in the greensynthesis of silver nanoparticles mediated by fig (Ficus carica) leaf extract. Spectrochim Acta A Mol Biomol Spectrosc 135:153–161

29. Li L, Sun J, Li X, Zhang Y, Wang Z, Wang C, Dai J, Wang Q (2012) Controllable synthesis of monodispersed silver nanoparticles as standards for quantitative assessment of their cytotoxicity. Biomaterials 33(6):1714–1721

30. Foldbjerg R, Dang DA, Autrup H (2011) Cytotoxicity and genotoxicity of silvernanoparticles in the human lung cancer cell line, A549. Arch Toxicol 85(7):743–750

31. Palaniappan P, Sathishkumar G, Sankar R (2015) Fabrication of nano-silver particles using Cymodocea serrulata and its cytotoxicity effect against human lung cancer A549 cells line. Spectrochim Acta A Mol Biomol Spectrosc 138:885–890

32. Vivek R, Thangam R, Muthuchelian K, Gunasekaran P, Kaveri K, Kannan S (2012) Green biosynthesis of silver nanoparticles from Annona squamosa leaf extract and its in vitro cytotoxic effect on MCF-7 cells. Process Biochem 47(12):2405–2410

33. Jeyaraj M, Rajesh M, Arun R, MubarakAli D, Sathishkumar G, Sivanandhan G, Dev GK, Manickavasagam M, Premkumar K, Thajuddin N, Ganapathi A (2013) An investigation on the cytotoxicity and caspase-mediated apoptotic effect of biologicallysynthesized silver nanoparticles using Podophyllum hexandrum on human cervicalcarcinoma cells. Colloids Surf B: Biointerfaces 102:708–717

34. Singh G, Babele PK, Shahi SK, Sinha RP, Tyagi MB, Kumar A (2014) Green synthesis of silver nanoparticles using cell extracts of Anabaena doliolum and screening of its antibacterial and antitumor activity. J Microbiol Biotechnol 24(10):1354–1367

35. Guo D, Dou D, Ge L, Huang Z, Wang L, Nb G (2015) A caffeic acid mediated facile synthesis of silver nanoparticles with powerful anti-cancer activity. Colloids Surf B: Biointerfaces 1(134): 229–234

36. Barabadi H, Alizadeh A, Ovais M, Ahmadi A, Shinwari ZK, Saravanan M (2018) Efficacy of green nanoparticles against cancerous and normal cell lines: a systematicreview and meta-analysis. IET Nanobiotechnol 12(4):377–391

37. He Y, Du Z, Ma S, Cheng S, Jiang S, Liu Y, Li D, Huang H, Zhang K, Zheng X (2016) Biosynthesis, antibacterial activity and anticancer effects against prostate cancer (PC-3) cells of silver nanoparticles using Dimocarpus Longan Lour. PeelExtract. Nanoscale Res Lett 11(1):300

38. Otsuki N, Dang NH, Kumagai E, Kondo A, Iwata S, Morimoto C (2010) Aqueous extract ofCarica papaya leaves exhibits anti-tumor activity and immunomodulatory effects. J Ethnopharmacol 127(3): 760–767

39. Nguyen TT, Parat MO, Hodson MP, Pan J, Shaw PN, Hewavitharana AK (2015) Chemical characterization and in vitro cytotoxicity on squamous cell carcinoma cells of Carica papaya leaf extracts. Toxins (Basel) 8(1):7

40. Banala RR, Nagati VB, Karnati PR (2015) Green synthesis and characterization of Carica papaya leaf extract coated silver

nanoparticles through X-ray diffraction, electron microscopy and evaluation of bactericidal properties. Saudi J Biol Sci 22(5):637–644

41. Pandian AM, Karthikeyan C, Rajasimman M, Dinesh MG (2015) Synthesis of silver nanoparticle and its application. Ecotoxicol Environ Saf 121:211–217

42. Mishra A, Sardar M (2015) Cellulase assisted synthesis of nano-silver and gold: application as immobilization matrix for biocatalysis. Int J Biol Macromol 77:105–113

43. Dong F, Valsami-Jones E, Kreft JU (2016) New, rapid method to measure dissolved silver concentration in silver nanoparticle suspensions by aggregation combined with centrifugation. J Nanopart Res 18(9):259

44. Mishra A, Kaushik NK, Sardar M, Sahal D (2013) Evaluation of antiplasmodial activity of green synthesized silver nanoparticles. Colloids Surf B: Biointerfaces 111:713–718

45. Singh DP, Gadi R, Mandal TK (2011) Characterization of particulate-bound polycyclic aromatic hydrocarbons and trace metals composition of urban air in Delhi, India. Atmos Environ 45(40):7653–7663

46. Nambiar D, Prajapati V, Agarwal R, Singh RP (2013) In vitro and in vivo anticancerefficacy of silibinin against human pancreatic cancer BxPC-3 and PANC-1 cells. Cancer Lett 334(1):109–117

47. Prajapati V, Kale RK, Singh RP (2015) Silibinin combination with arsenic strongly inhibits survival and invasiveness of human prostate carcinoma cells. Nutr Cancer 67(4):647–658

48. Kumar K, Mishra JPN, Singh RP (2020) Usnic acid induces apoptosis in human gastriccancer cells through ROS generation and DNA damage and causes up-regulation ofDNA-PKcs and γ-H2A.X phosphorylation. Chem Biol Interact 315:108898

49. Raju J, Patlolla JM, Swamy MV, Rao CV (2004) Diosgenin, a steroid saponin of Trigonella foenum graecum (fenugreek), inhibits azoxymethane-induced aberrant crypt foci formation in F344 rats and induces apoptosis in HT-29 human colon cancer cells. Cancer Epidemiol Biomark Prev 13(8):1392–1398

50. Shyanti RK, Sehrawat A, Singh SV, Mishra JPN, Singh RP (2017) Zerumbone modulatesCD1d expression and lipid antigen presentation pathway in breast cancer cells. Toxicol in Vitro 44:74–84

51. Verma A, Mehata MS (2016) Controllable synthesis of silver nanoparticles using Neem leaves and their antimicrobial activity. J Radiat Res Appl Sci 9(1):109–115

52. Tripathy A, Raichur AM, Chandrasekaran N, Prathna TC, Mukherjee A (2010) Process variables in biomimetic synthesis of silver nanoparticles by aqueous extract of Azadirachta indica (Neem) leaves. J Nanopart Res 12(1):237–246

53. Pimprikar PS, Joshi SS, Kumar AR, Zinjarde SS, Kulkarni SK (2009) Influence ofbiomass and gold salt concentration on nano-particle synthesis by the tropicalmarine yeast Yarrowia lipolytica NCIM 3589. Colloids Surf B: Biointerfaces 74(1):309–316

54. Roopan SM, Madhumitha G, Rahuman AA, Kamaraj C, Bharathi A, Surendra TV (2013) Low-cost and eco-friendly phyto-synthesis of silver nanoparticles using Cocos nucifera coir extract and its larvicidal activity. Ind Crop Prod 43:631–635

55. Banerjee P, Satapathy M, Mukhopahayay A, Das P (2014) Leaf extract mediated green synthesis of silver nanoparticles from widely available Indian plants: synthesis, characterization, antimicrobial property and toxicity analysis. Bioresour Bioprocess 1(1):1-10

56. Shankar SS, Rai A, Ahmad A, Sastry M (2004) Rapid synthesis of Au, Ag, andbimetallic Au core-Ag shell nanoparticles using Neem (Azadirachta indica) leaf broth. J Colloid Interface Sci 275(2):496–502

57. Gan PP, Ng SH, Huang Y, Li SF (2012) Green synthesis of gold nanoparticles usingpalm oil mill effluent (POME): a low-cost and eco-friendly viable approach. Bioresour Technol 113:132–135

58. Kathiravan V, Ravi S, Ashokkumar S, Velmurugan S, Elumalai K, Khatiwada CP (2015) Green synthesis of silver nanoparticles using Croton sparsiflorus morong leaf extract and their antibacterial and antifungal activities. Spectrochim Acta A Mol Biomol Spectrosc 139:200–205

59. Maddinedi SB, Mandal BK, Patil SH, Andhalkar VV, Ranjan S, Dasgupta N (2017) Diastase induced green synthesis of bilayered reduced graphene oxide and itsdecoration with gold nanoparticles. J Photochem Photobiol B 166:252–258

60. Sabarwal A, Agarwal R, Singh RP (2017) Fisetin inhibits cellular proliferation and induces mitochondria-dependent apoptosis in human gastric cancer cells. Mol Carcinog 56(2):499–514

61. Salunke BK, Shin J, Sawant SS, Alkotaini B, Lee S, Kim BS (2014) Rapid biological synthesis of silver nanoparticles using Kalopanax pictus plant extract and their antimicrobial activity. Korean J Chem Eng 31(11):2035–2040

62. Maddinedi SB, Mandal BK, Anna KK (2017) Tyrosine assisted size controlled synthesis of silver nanoparticles and their catalytic, in-vitro cytotoxicity evaluation. Environ Toxicol Pharmacol 51:23–29

63. Barabadi H, Vahidi H, Kamali KD, Rashedi M, Hosseini O, Ghomi AR, Saravanan M (2020) Emerging theranostic silver nanomaterials to combat colorectal cancer: a systematic review. J Clust Sci 31:311–321

64. Barabadi H, Najafi M, Samadian H, Azarnezhad A, Vahidi H, Mahjoub MA, KoohiyanM AA (2015) A systematic review of the genotoxicity and antigenotoxicity of biologically synthesized metallic nanomaterials: are green nanoparticles safe enough for clinical marketing? Medicina (Kaunas) 55(8):439

65. Mortezaee K, Najafi M, Samadian H, Barabadi H, Azarnezhad A, Ahmadi A (2019) Redox interactions and genotoxicity of metal-based nanoparticles: a comprehensive review. Chem Biol Interact 312:108814

66. Akhtar MJ, Alhadlaq HA, Alshamsan A, Majeed Khan MA, Ahamed M (2015) Aluminum doping tunes band gap energy level as well as oxidative stress-mediated cytotoxicity of ZnO nanoparticles in MCF-7 cells. Sci Rep 5:13876

67. Krishna KL, Paridhavi M, Patel JA (2008) Review on nutritional, medicinal and pharmacological properties of Papaya (Carica papaya Linn.). Nat Prod Radiance 7(4):364–373

68. Rodríguez-León E, Iñiguez-Palomares R, Navarro RE, Herrera-Urbina R, Tánori J, Iñiguez-Palomares C, Maldonado A (2013) Synthesis of silver nanoparticles using reducing agents obtained from natural sources (Rumex hymenosepalus extracts). Nanoscale Res Lett 8(1):318

69. Abreu Velez AM, Howard MS (2015) Tumor-suppressor genes, cell cycle regulatory checkpoints, and the skin. N Am J Med Sci 7(5):176–188

70. Li S, Wang C, Yu X, Wu H, Hu J, Wang S, Ye Z (2017) miR-3619-5p inhibits prostate cancer cell growth by activating CDKN1A expression. Oncol Rep 37(1):241–248

71. Yim D, Singh RP, Agarwal C, Lee S, Chi H, Agarwal R (2005) A novel anticancer agent, decursin, induces G1 arrest and apoptosis in human prostate carcinoma cells. Cancer Res 65(3):1035–1044

72. Roy S, Gu M, Ramasamy K, Singh RP, Agarwal C, Siriwardana S, Sclafani RA, Agarwal R (2009) p21/Cip1 and p27/Kip1 are essential molecular targets of inositolhexaphosphate for its anti-tumor efficacy against prostate cancer. Cancer Res 69(3):1166–1173

73. Roy S, Singh RP, Agarwal C, Siriwardana S, Sclafani R, Agarwal R (2008) Downregulation of both p21/Cip1 and p27/Kip1 produces a more aggressive prostate cancer phenotype. Cell Cycle 7(12):1828–1835

74. Dewaele M, Maes H, Agostinis P (2010) ROS-mediated mechanisms of autophagystimulation and their relevance in cancer therapy. Autophagy 6(7):838–854

75. Singh RP, Tyagi A, Sharma G, Mohan S, Agarwal R (2008) Oral silibinin inhibits in vivo human bladder tumor xenograft growth involving down-regulation of survivin. Clin Cancer Res 14(1): 300–308

76. Jaiswal A, Sabarwal A, Mishra JP, Singh RP (2018) Plumbagin induces ROS-mediated apoptosis and cell cycle arrest and inhibits EMT in human cervical carcinoma cells. RSC Adv 8(56):32022–32037